ELSEVIER

15 April 1996

Optics Communications 125 (1996) 302–323

OPTICS COMMUNICATIONS

Full length article

Spiral-type beams: optical and quantum aspects

E. Abramochkin [1], V. Volostnikov [1]

Lebedev Physics Institute, Russian Academy of Sciences, Novo-Sadovaya Street 221, Samara 443011, Russia

Received 27 June 1995

Abstract

The existence of spiral-type beams with a predetermined intensity distribution is investigated by theoretical and experimental means. Spiral-type beams with an intensity distribution in the form of an arbitrary planar line were found. A correspondence between these laser beams and a specific quantum-mechanical situation — ground states of a charged particle in a uniform magnetic field — was found. The connection between spiral-type beams and coherent states is shown. Some methods of spiral-type beam synthesis are described. Experimental results of transformation of a gaussian beam into a triangle-line laser beam are presented.

1. Introduction

It is well known from publications on the phase-retrieval problem that relations between intensity and phase in one-dimensional and two-dimensional cases are essentially different. The physical aspects of this difference have been investigated in Refs. [1–3]. As has been shown there, the difference is closely connected to the possibility of the appearance of a vortical component of the energy flux field in the two-dimensional case. A nonzero curl of the energy flux field makes the relation between intensity and phase much more complicated in this case. On the other hand, this complexity is a source of new possibilities. In the two-dimensional case there is, in the paraxial approximation, a family of so-called spiral-type beams: vortical wave fields that leave the intensity unchanged under propagation and focusing, if we neglect scale and rotation [4]. In particular, these wave fields have been found as a generalization of gaussian beams in the form

$$F(x, y, l) = \frac{1}{\sigma} \exp\left(-\frac{x^2+y^2}{\rho^2\sigma}\right) f\left(\frac{x \pm \mathrm{i}y}{\rho\sigma}\right), \tag{1}$$

where $f(z)$ is an arbitrary analytic entire function, $\sigma = 1 + 2\mathrm{i}l/k\rho^2$, l is a distance along the direction of propagation of the beam, $\rho = \text{const}$, k is a wave number and the argument sign of $f(z)$ determines the rotation direction relative to the propagation direction.

[1] E-mail: root@fian.samara.su.

0030-4018/96/$12.00 © 1996 Elsevier Science B.V. All rights reserved
SSDI 0030-4018(95)00640-0

It is seen from the given formula that the wave field family is extensive enough but the question of existence for a beam with predetermined intensity and constructive way to select it from the family is a non-trivial problem.

In this paper we study some possibilities to create beams with a structurally stable intensity distribution under propagation and focusing. The beams found have various intensities and may be applicable in laser technology.

Our paper is organized as follows. In Section 2, general properties of spiral-type beams are considered and some simple beams are constructed on this basis. In Section 3 the problem of construction of more general spiral-type beams with the topology of an arbitrary planar curve is investigated. In Section 4 some properties of beams for closed curves and the quantum-mechanical aspects of the results found are presented. In Section 5 we deal with methods of realization of various spiral-type beams; experimental results are presented in the same section. The results of the paper are discussed in Section 6.

2. Spiral-type beam properties and simple beams

As the intensity of a spiral-type beam (1) is structurally stable for all l, it is sufficient to consider them at the waist plane $l=0$ ($\sigma=1$) with positive sign in the argument of function f only. Let us define

$$\mathcal{S}(z,\bar{z}) = \exp(-z\bar{z}/\rho^2) f(z/\rho), \tag{2}$$

where $z=x+\mathrm{i}y$, $\bar{z}=x-\mathrm{i}y$ are complex variables. Then $\mathcal{S}(z,\bar{z})$ gives a complete description of the $F(x, y, l)$ in plane $l=0$ and its evolution under propagation. So, we will refer to $\mathcal{S}(z,\bar{z})$ as the spiral-type beam (1).

Let us consider some general properties of the spiral-type beam family, which are deduced from (2) and will be used below.

Property A. If $\mathcal{S}_n(z,\bar{z}) = \exp(-z\bar{z}/\rho^2) f_n(z/\rho)$ is a set of spiral-type beams, then a linear combination $\mathcal{S}(z,\bar{z}) = \sum_n c_n \mathcal{S}_n(z,\bar{z})$ is a spiral-type beam. More generally, if $\mathcal{S}(z,\bar{z},a) = \exp(-z\bar{z}/\rho^2) f(z/\rho, a)$ is a spiral-type beam dependent on parameter a, then $\mathcal{S}(z,\bar{z}) = \int \mathcal{S}(z,\bar{z},a)\,\mathrm{d}a$ is also a spiral-type beam.

Property B. If $\mathcal{S}_0(z,\bar{z}) = \exp(-z\bar{z}/\rho^2) f(z/\rho)$ is a spiral-type beam, then $\mathcal{S}(z,\bar{z}) = \exp(-z\bar{z}/\rho^2) \times f(z\mathrm{e}^{-\mathrm{i}\alpha}/\rho)$ is a spiral-type beam whose intensity is the same as that of $\mathcal{S}_0(z,\bar{z})$, but rotated over an angle α.

Property C. If $\mathcal{S}_0(z,\bar{z}) = \exp(-z\bar{z}/\rho^2) f(z/\rho)$ is a spiral-type beam, then

$$\mathcal{S}(z,\bar{z}) = \exp\left[-\left(z\bar{z} - 2z\bar{z}_0 + z_0\bar{z}_0\right)/\rho^2\right] f((z-z_0)/\rho) \tag{3}$$

is a spiral-type beam whose intensity is the same as that of $\mathcal{S}_0(z,\bar{z})$, but displaced to the point z_0. In this case, in contrast with the previous one, substitution of the variable $z \mapsto z - z_0$ does not lead to the desired result immediately. It is easy to see that

$$\exp\left(-\frac{(z-z_0)(\bar{z}-\bar{z}_0)}{\rho^2}\right) f\left(\frac{z-z_0}{\rho}\right) = \exp\left(-\frac{z\bar{z} - \bar{z}z_0 - z\bar{z}_0 + z_0\bar{z}_0}{\rho^2}\right) f\left(\frac{z-z_0}{\rho}\right)$$

is not a spiral-type beam because of the factor $\exp(\bar{z}z_0/\rho^2)$. Multiplying it by a linear phase function $\exp(-(\bar{z}z_0 - z\bar{z}_0)/\rho^2)$ we keep the intensity distribution and obtain the requested spiral-type beam.

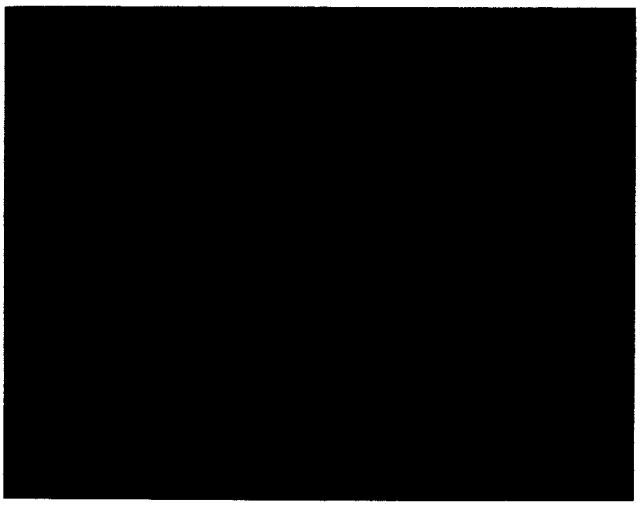

Fig. 1. Trajectories of maximum points of gaussian beams $\mathscr{S}_{z_0}(z, \bar{z})$ — straight lines — at $|z_0| = \text{const}$ are placed on the hyperboloid surface.

From Eq. (3) for $f(z) \equiv 1$ we have an "elementary" spiral-type beam

$$\mathscr{S}_{z_0}(z, \bar{z}) = \exp\left[-\left(z\bar{z} - 2z\bar{z}_0 + z_0\bar{z}_0\right)/\rho^2\right], \tag{4}$$

with gaussian intensity distribution displaced to the point z_0 [2]. The beam phase is a linear function of coordinates and, of course, the beam propagates along a straight line. In this connection it is instructive to consider how the beam rotation occurs under propagation. From Eq. (1) it follows that the trajectory of the point of maximum intensity of the beam (4) in (x, y, l) space is described by the expression

$$x + \mathrm{i}y = z_0|\sigma|\exp[\mathrm{i}\arg(\sigma)] = (x_0 + \mathrm{i}y_0)(1 + 2\mathrm{i}l/k\rho^2), \tag{5}$$

where x_0, y_0 are the coordinates of the point of maximum intensity z_0 at $l = 0$.

Let us consider the beam family (4) for $|z_0| = \text{const}$. From (5) it is seen that the trajectories of the maximum intensity point of these beams form a hyperboloid of one sheet in (x, y, l) space:

$$x^2 + y^2 - \frac{4|z_0|^2}{k^2\rho^4}l^2 = |z_0|^2.$$

The maximum-point trajectories for some beams on the hyperboloid surface are shown in Fig. 1. As for general spiral-type beams (see Ref. [4]), trajectories starting from z_0 on plane $l = 0$ are on the same hyperboloid and are generally spirals.

Using Property A to sum displaced gaussian beams (4) makes it possible to form various spiral-type beams.

[2] Spiral-type beams can be compared with coherent states $|\alpha\rangle$ in quantum mechanics and paraxial optics [5]. For example, the scalar product of "elementary" spiral-type beams in the space $L_2(\mathbb{R}^2)$ $(\mathscr{S}_{z_0}, \mathscr{S}_{z_1}) = \frac{1}{2}\pi\rho^2\exp(-(|z_0|^2 - 2\bar{z}_0 z_1 + |z_1|^2)/\rho^2)$ is similar to the scalar product of coherent states $\langle\alpha|\beta\rangle = \exp(-\frac{1}{2}(|\alpha|^2 - 2\bar{\alpha}\beta + |\beta|^2))$. In a more general way, if $\mathscr{S}(z, \bar{z}) = \exp(-z\bar{z}/\rho^2)\psi(z/\rho)$ is a spiral-type beam, then $(\mathscr{S}, \mathscr{S}_{z_0}) = \frac{1}{2}\pi\rho^2\mathscr{S}(z_0)$. For coherent states this is similar to $\langle\alpha|\psi\rangle = \exp(-\frac{1}{2}|\alpha|^2)\psi(\bar{\alpha})$, where $|\psi\rangle = \sum_{n=0}^{\infty} c_n|n\rangle$. The connection between the astigmatic transformation of spiral-type beams and coherent states in coordinate and Fock–Bargman representations is shown in Appendix B.

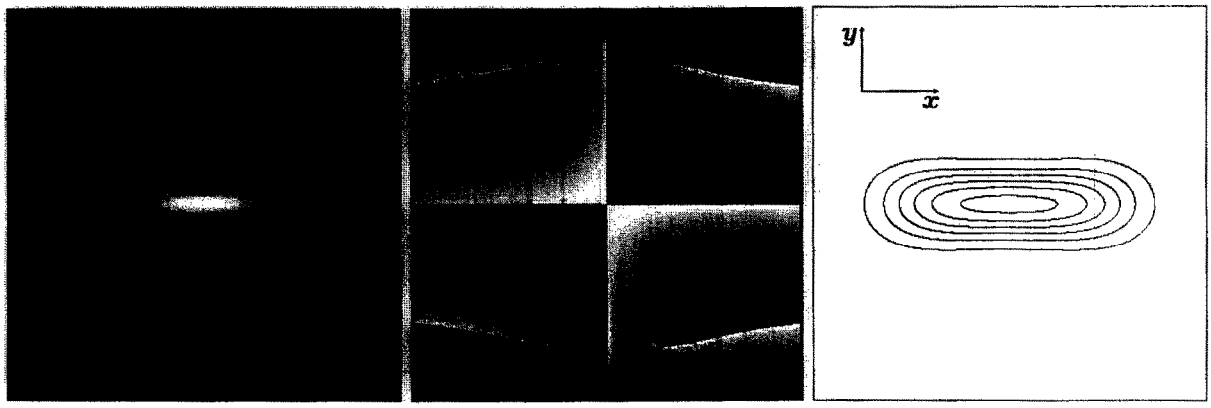

a b c

Fig. 2. Intensity (a), phase (b), and intensity level contours (c) of a spiral-type beam in the form of segment $[-T, T]$. In the phase pattern black corresponds to phase $\varphi = 0$ and white to phase $\varphi = 2\pi$. The presence of six wave front dislocations in isolated zeros of the intensity is seen.

A simple example of this kind that corresponds to uniformly dense filling of the segment $[-T, T]$ in the complex plane by beams (4) is

$$\mathscr{S}(z, \bar{z}|[-T, T]) = \exp\left(-\frac{z\bar{z}}{\rho^2}\right)\int_{-T}^{T}\exp\left(-\frac{t^2}{\rho^2}+\frac{2zt}{\rho^2}\right)\mathrm{d}t. \tag{6}$$

Intensity distribution, phase distribution and intensity level contours for this beam are shown in Fig. 2. The orientation of the coordinate axes is shown in Fig. 2c. (This wavefield and subsequent ones were calculated using numerical methods.) The beam intensity has a gaussian decrease in any direction outside the segment $[-T, T]$ and at $\rho \ll T$ almost all energy is concentrated in a small neighborhood of this segment.

From (6), with the help of Properties B and C, it is easy to obtain the spiral-type beam which has an intensity distribution in the shape of an arbitrary segment in the complex plane. Let us determine $z_0 = \frac{1}{2}(z_1 + z_2)$, $T = \frac{1}{2}|z_2 - z_1|$ and $\alpha = \arg(z_2 - z_1)$. Then the mapping $z \mapsto z_0 + ze^{i\alpha}$ transforms the segment $[-T, T]$ into the segment $[z_1, z_2]$. Hence, the beam for $[z_1, z_2]$ has the form of

$$\mathscr{S}(z, \bar{z}|[z_1, z_2]) = \exp\left(-\frac{z\bar{z}-2z\bar{z}_0+z_0\bar{z}_0}{\rho^2}\right)\int_{-T}^{T}\exp\left(-\frac{t^2}{\rho^2}+\frac{2(z-z_0)\,e^{-i\alpha}t}{\rho^2}\right)\mathrm{d}t. \tag{7}$$

We will name $[z_1, z_2]$ the generating segment for the beam (7). On the straight line containing the segment $[z_1, z_2]$, the beam complex amplitude in the point $z_c = cz_1 + (1-c)z_2$ is

$$\mathscr{S}(z_c, \bar{z}_c|[z_1, z_2]) = \exp\left[i(2c-1)\,\mathrm{Im}(z_1\bar{z}_2)/\rho^2\right]\int_{-c|z_2-z_1|}^{(1-c)|z_2-z_1|}\exp(-t^2/\rho^2)\,\mathrm{d}t.$$

Thus, the beam values $\mathscr{S}(z, \bar{z}|[z_1, z_2])$ are complex conjugates in points of the line $z = cz_1 + (1-c)z_2$, which are symmetrically located with respect to the point $\frac{1}{2}(z_1 + z_2)$. In particular, in the boundary points of segment $[z_1, z_2]$,

$$\mathscr{S}(z_1, \bar{z}_1|[z_1, z_2]) = \overline{\mathscr{S}}(z_2, \bar{z}_2|[z_1, z_2]) = \exp\left(i\,\mathrm{Im}(z_1\bar{z}_2)/\rho^2\right)\int_0^{|z_2-z_1|}\exp(-t^2/\rho^2)\,\mathrm{d}t. \tag{8}$$

Due to the strong localization of beams (7) at $\rho \ll T$ in the vicinity of their generating segments, the interference of these beams is weak, if they are distant from each other. Owing to this property, the intensity distribution of the field, which is the sum of these beams, is similar to the sum of their intensities.

Consider now two adjoining segments $[a, b]$ and $[b, c]$ on the real axis. Then the spiral-type beams $\mathscr{S}(z, \bar{z}|[a, b])$ and $\mathscr{S}(z, \bar{z}|[b, c])$ join seamlessly:

$$\mathscr{S}(z, \bar{z}|[a, c]) = \mathscr{S}(z, \bar{z}|[a, b]) + \mathscr{S}(z, \bar{z}|[b, c]).$$

In general, when two segments $[z_1, z_2]$, $[z_2, z_3]$ lie on the same straight line, from definition (7) it follows that the analogous smooth junction of the beams $\mathscr{S}(z, \bar{z}|[z_1, z_2])$ and $\mathscr{S}(z, \bar{z}|[z_2, z_3])$ has the form

$$\mathscr{S}(z, \bar{z}|[z_1, z_3]) = \exp(-\mathrm{i}\,\mathrm{Im}(\bar{z}_2 z_3)/\rho^2)\mathscr{S}(z, \bar{z}|[z_1, z_2]) + \exp(-\mathrm{i}\,\mathrm{Im}(\bar{z}_2 z_1)/\rho^2)\mathscr{S}(z, \bar{z}|[z_2, z_3]). \tag{9}$$

Therefore, this case, in contrast with the previous one, needs phase agreement between the summand beams. From Eqs. (8), (9) it follows that the phases of summands in the junction point z_2 are equal:

$$\arg[\exp(-\mathrm{i}\,\mathrm{Im}(\bar{z}_2 z_3)/\rho^2)\mathscr{S}(z_2, \bar{z}_2|[z_1, z_2])] = \arg[\exp(-\mathrm{i}\,\mathrm{Im}(\bar{z}_2 z_1)/\rho^2)\mathscr{S}(z_2, \bar{z}_2|[z_2, z_3])].$$

So, if one considers the beam $\mathscr{S}(z, \bar{z}|[z_1, z_2]) + \mathrm{e}^{\mathrm{i}\varphi}\,\mathscr{S}(z, \bar{z}|[z_2, z_3])$ for $\varphi \in [0, 2\pi]$, then uniformity of the sum intensity distribution along the segment $[z_1, z_3]$ is best at

$$\varphi = \arg\,\mathscr{S}(z_2, \bar{z}_2|[z_1, z_2]) - \arg\,\mathscr{S}(z_2, \bar{z}_2|[z_2, z_3]) = \mathrm{Im}(\bar{z}_2(z_3 - z_1))/\rho^2 \tag{10}$$

and Eq. (10) may be considered as an optimum condition to make the intensity distribution uniform for the junction of two "segment"-beams if points z_1, z_2, z_3 are on a straight line [3].

Let now the points z_1, z_2, z_3 not be on a straight line. In this case interdependence of the "segment"-beams is essential in the vicinity of point z_2, so we have a reason to apply the phase agreement concept (10) to construct a spiral-type beam in the shape of the broken line $[z_1, z_2] \cup [z_2, z_3]$. Numerical experiments show that the intensity distribution of the beam

$$\mathscr{S}(z, \bar{z}|[z_1, z_2] \cup [z_2, z_3]) = \mathscr{S}(z, \bar{z}|[z_1, z_2]) + \exp(\mathrm{i}\,\mathrm{Im}(\bar{z}_2(z_3 - z_1))/\rho^2)\mathscr{S}(z, \bar{z}|[z_2, z_3]) \tag{11}$$

along the broken generating line is uniform enough for various values of the angle between components $[z_1, z_2]$ and $[z_2, z_3]$. Thus, the phase agreement principle is helpful to build spiral-type beams shaped as various broken lines. The generalization of Eq. (11) to polygonal lines is not difficult.

Based on the fields presented in this section it is possible to construct spiral-type beams with rather varied topologies. A field example containing all kinds of the basic beams is given in Fig. 3.

3. General type beams

The results of the previous section naturally raise the following question. Let $\zeta(t)$ be an arbitrary planar curve, represented in complex-valued form, and parameter t run from 0 to T. Is there a spiral-type beam $\mathscr{S}(z, \bar{z}|\,\zeta(t), t \in [0, T])$ shaped like this curve? Of course, the expression "beam shaped like the curve $\zeta(t)$" demands a selection criterion but here we will not define more exactly the mathematical statement, assuming that the desired result is visually similar. That is, the beam intensity must be as large as possible in points of the curve $\zeta(t)$ and as small as possible in other points of the plane.

We will construct a spiral-type beam $\mathscr{S}(z, \bar{z}|\,\zeta(t), t \in [0, T])$ as the limiting case of beams that realize

[3] It should be noted that Eq. (10) may be written with an additional summand $2\pi N$ (N is an integer), since it connects arguments of complex exponential functions.

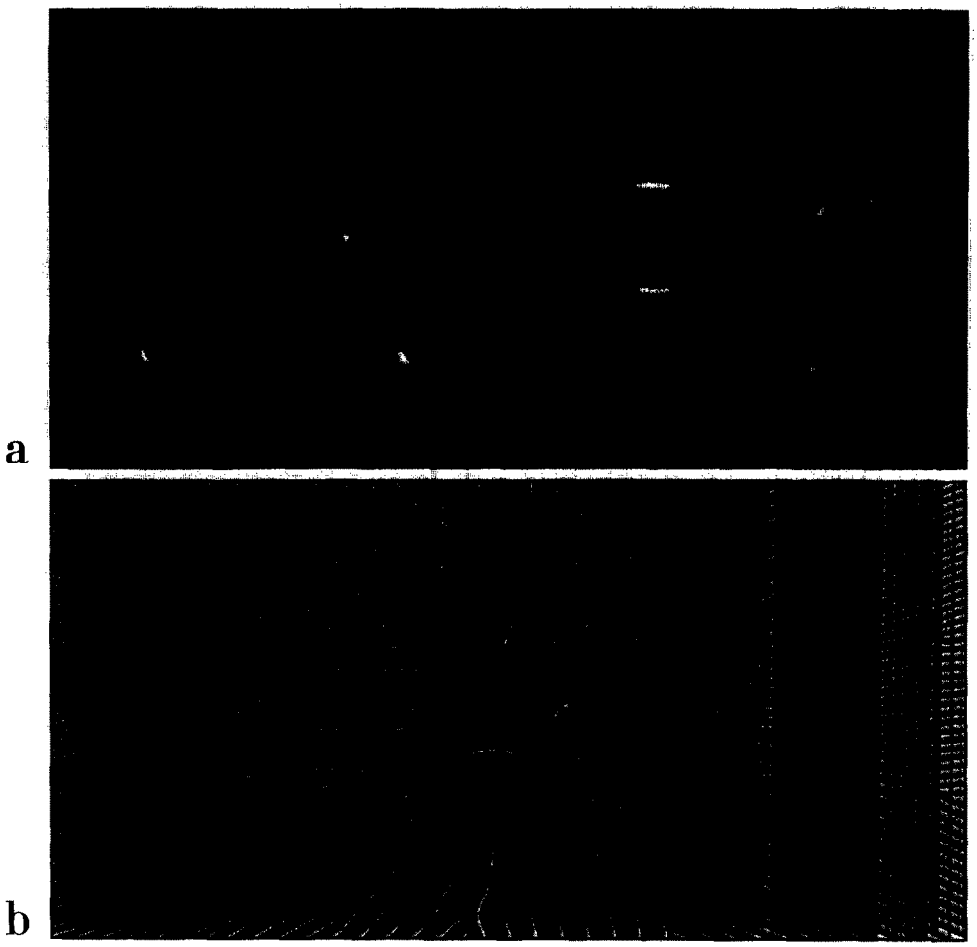

Fig. 3. Intensity (a) and phase (b) of the beam, which is a sum of simple spiral-type beams.

approximating polygonal lines for $\zeta(t)$. Let parameter t of the curve $\zeta(t)$ run from 0 to T, $\{kT/n;\ k=0,\ 1,\ldots,\ n\}$ be a partition of the segment $[0,\ T]$ and $\{\zeta_k=\zeta(kT/n);\ k=0,\ 1,\ldots,\ n\}$ be a corresponding partition of the curve $\zeta(t)$ (see Fig. 4). Then the polygonal line

$$\bigcup_{k=0}^{n-1}[\zeta_k,\ \zeta_{k+1}]=[\zeta_0,\ \zeta_1]\cup[\zeta_1,\ \zeta_2]\cup\ldots\cup[\zeta_{n-1},\ \zeta_n]$$

approximates the curve $\zeta(t)$ and the corresponding "segment"-beams $\mathscr{S}(z,\ \bar{z}|[\zeta_k,\ \zeta_{k+1}])$ realize individual components of the line.

Using representation (11) for a broken-line beam, let us construct an approximating spiral-type beam:

$$\mathscr{S}\left(z,\ \bar{z}|\ \bigcup_{k=0}^{n-1}[\zeta_k,\ \zeta_{k+1}]\right)=\sum_{k=0}^{n-1}e^{i\varphi_k}\,\mathscr{S}(z,\ \bar{z}|[\zeta_k,\ \zeta_{k+1}]). \tag{12}$$

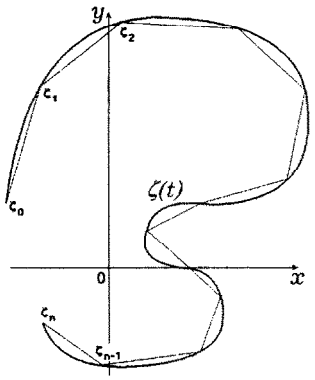

Fig. 4. A curve $\zeta(t)$ and its approximating polygonal line.

Here $\varphi_0 = 0$ and other constants φ_k are used for phase agreement in the points ζ_k. For each beam pair whose generating segments have a common point, the phase agreement condition is presented by

$$\varphi_{k-1} + \arg \mathscr{S}\left(\zeta_k, \bar{\zeta}_k \,|[\zeta_{k-1}, \zeta_k]\right) = \varphi_k + \arg \mathscr{S}\left(\zeta_k, \bar{\zeta}_k \,|[\zeta_k, \zeta_{k+1}]\right), \qquad k = 1, \ldots, n-1.$$

Using Eq. (8), we obtain the following solution of the system:

$$\varphi_k = \sum_{j=1}^{k} \left[\arg \mathscr{S}\left(\zeta_j, \bar{\zeta}_j \,|[\zeta_{j-1}, \zeta_j]\right) - \arg \mathscr{S}\left(\zeta_j, \bar{\zeta}_j \,|[\zeta_j, \zeta_{j+1}]\right)\right]$$

$$= \frac{1}{2i\rho^2} \sum_{j=1}^{k} \left[\bar{\zeta}_j\left(\zeta_{j+1} - \zeta_{j-1}\right) - \zeta_j\left(\bar{\zeta}_{j+1} - \bar{\zeta}_{j-1}\right)\right], \qquad k = 1, \ldots, n-1.$$

Substituting these expressions into Eq. (12) and reducing the length of each polygonal line component to zero, we have

$$\mathscr{S}(z, \bar{z} \,|\, \zeta(t), t \in [0, T])$$

$$= \lim_{n\to\infty} \mathscr{S}\left(z, \bar{z} \,|\, \bigcup_{k=0}^{n-1} [\zeta_k, \zeta_{k+1}]\right)$$

$$= \lim_{n\to\infty} \sum_{k=0}^{n-1} \left\{ \exp\left[\frac{1}{\rho^2 n} \sum_{j=1}^{k} \left(\bar{\zeta}_j \frac{\zeta_{j+1} - \zeta_{j-1}}{2/n} - \zeta_j \frac{\bar{\zeta}_{j+1} - \bar{\zeta}_{j-1}}{2/n}\right)\right] \exp\left[-\frac{z\bar{z}}{\rho^2} - \frac{|\zeta_k + \zeta_{k+1}|^2}{4\rho^2}\right.\right.$$

$$\left.\left. + \frac{z\left(\bar{\zeta}_k + \bar{\zeta}_{k+1}\right)}{\rho^2}\right] \int_{-\frac{1}{2}|\zeta_{k+1} - \zeta_k|}^{\frac{1}{2}|\zeta_{k+1} - \zeta_k|} \exp\left(-\frac{t^2}{\rho^2} + \frac{t(2z - \zeta_k - \zeta_{k+1})e^{-i\arg(\zeta_{k+1} - \zeta_k)}}{\rho^2}\right) dt \right\}$$

$$= \exp\left(-\frac{z\bar{z}}{\rho^2}\right) \lim_{n\to\infty} \frac{1}{n} \sum_{k=0}^{n-1} \left\{ \exp\left[\frac{1}{\rho^2 n} \sum_{j=1}^{k} \left(\bar{\zeta}_j \frac{\zeta_{j+1} - \zeta_{j-1}}{2/n} - \zeta_j \frac{\bar{\zeta}_{j+1} - \bar{\zeta}_{j-1}}{2/n}\right)\right]\right.$$

$$\left. \times \exp\left(-\frac{1}{\rho^2}\left(\zeta_k \bar{\zeta}_k - 2z\bar{\zeta}_k\right)\right) \frac{|\zeta_{k+1} - \zeta_k|}{1/n} \right\}.$$

Considering the given limit as that of the integral sum, we obtain

$$\mathscr{S}(z, \bar{z} \mid \zeta(t), t \in [0, T])$$

$$= \exp(-z\bar{z}/\rho^2) \int_0^T \exp\left[-\frac{\zeta(t)\bar{\zeta}(t)}{\rho^2} + \frac{2z\bar{\zeta}(t)}{\rho^2} + \frac{1}{\rho^2} \int_0^t \left(\bar{\zeta}(\tau)\zeta'(\tau) - \zeta(\tau)\bar{\zeta}'(\tau) \right) \mathrm{d}\tau \right] \mid \zeta'(t) \mid \mathrm{d}t. \tag{13}$$

Thus, we have built the spiral-type beam for the curve $\zeta(t)$. To what extent does its intensity distribution correspond to the shape of the curve? The beam representation (13) contains the curve invariants: the arc length differential, $|\zeta'(t)|\mathrm{d}t$, and the oriented area of sectorial domain, swept out under motion along the curve $[1/(4\mathrm{i})]\int_0^t (\bar{\zeta}\zeta' - \zeta\bar{\zeta}')\,\mathrm{d}\tau$. As a result, the beam is generated by the curve as a geometrical object in the plane. In particular, the beam does not depend on the parametrization of the curve. On the other hand, for the construction of the beam (13) the phase agreement principle has been used for two and only two adjoining components of the polygonal line, excluding other component's contributions. It is evident that when the polygonal line component length is reduced, the corresponding field length does not tend to zero and the field interdependence increases. Besides, the shape of the curve is essential. As an example, in Fig. 5 the intensity and phase of a spiral-type beam for an Archimedes spiral $\zeta(t) = te^{\mathrm{i}t}$ are shown. The spiral pitch was selected to demonstrate the interference between coils. The coil interdependence increases with decreasing pitch, since it becomes comparable with the gaussian parameter ρ.

For a closed curve $\zeta(t)$, $t \in [0, T]$, the interdependence arises under spiral-type beam construction for corresponding polygonal lines as an additional condition to adjust the phases of the first and the last links in the point $\zeta_0 = \zeta_n$.

Thus, the relation between a curve $\zeta(t)$ and a spiral-type beam (13) is generally not evident. Some aspects of the problem will be considered in the next section.

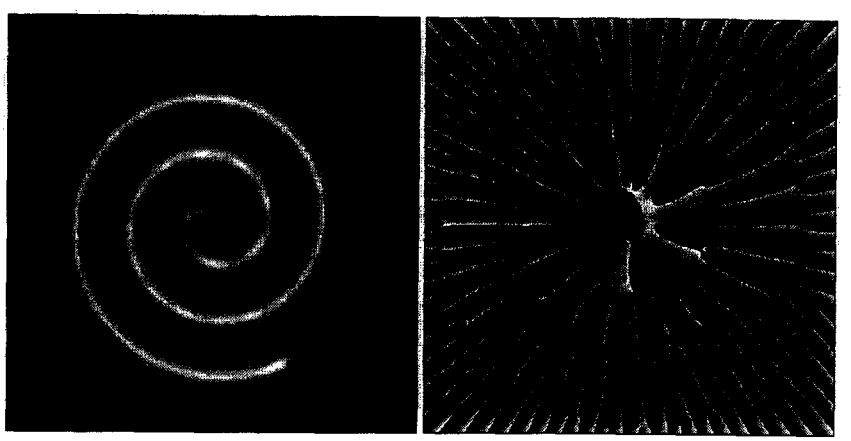

a b

Fig. 5. Intensity (a) and phase (b) of a beam in the form of the Archimedes spiral. Isolated zeros of the beam intensity are seen between coils.

4. Closed-curve beams

a) Quantization condition

Beams for closed curves are special ones and require individual consideration. Let function $\zeta(t)$, $t\in[0, T]$ describe a closed curve with no self-crossings. Without loss of generality we suppose that with growing t we move around the curve in the counter-clockwise direction. Let us define $\zeta(t)$ for all real t by continuing it periodically over the segment $[0, T]$. Then the functions $\zeta(t+a)$, $t\in[0, T]$ at various real a describe the same curve. Do the beams coincide for $\zeta(t+a)$ at various a? Here we show that the beams constructed for a closed curve show certain quantization properties. This is shown by the following facts: first, the beam intensity distribution changes radically under similarity transformation $\zeta(t)\to\nu\zeta(t)$ and takes the shape of the curve $\nu\zeta(t)$ at definite discrete values of ν only. Secondly, beam intensities are the same for $\nu\zeta(t+a)$ at various a at the very same values of ν only.

Now we will find the condition under which the spiral-type beams constructed for the curves $\zeta(t)$ and $\zeta(t+a)$ coincide:

$$|\mathscr{S}(z, \bar{z}\,|\,\zeta(t), t\in[a, a+T])|^2\equiv|\mathscr{S}(z, \bar{z}\,|\,\zeta(t), t\in[0, T])|^2.$$

This identity may be written in the form

$$e^{i\Phi(a)}\mathscr{S}(z, \bar{z}\,|\,\zeta(t), t\in[a, a+T])=\mathscr{S}(z, \bar{z}\,|\,\zeta(t), t\in[0, T]), \tag{14}$$

where $\Phi(a)$ is some real-valued function not depending on z (otherwise, removing the gaussian functions from both parts of Eq. (14), we have that Φ is an analytical function of z and, therefore, is not a real-valued function for all z). Differentiating Eq. (14) with respect to a and taking into account the periodicity of $\zeta(t)$, we have

$$e^{i\Phi(a)}\mathscr{S}(z, \bar{z}\,|\,\zeta(t), t\in[a, a+T])\left[i\Phi'(a)-\frac{\bar{\zeta}(a)\zeta'(a)-\zeta(a)\bar{\zeta}'(a)}{\rho^2}\right]$$

$$+\exp\left[i\Phi(a)-\frac{z\bar{z}-2z\bar{\zeta}(a)+\zeta(a)\bar{\zeta}(a)}{\rho^2}\right]\left[\exp\left(\frac{1}{\rho^2}\int_0^T\left(\bar{\zeta}\zeta'-\zeta\bar{\zeta}'\right)d\tau\right)-1\right]|\zeta'(a)|=0.$$

Substituting the spiral-type beam in this expression in accordance with Eq. (14) and removing gaussian factors, we represent this equation in symbolic form as:

$$f(z)F_1(a)+\exp\left(2z\bar{\zeta}(a)/\rho^2\right)F_2(a)=0,$$

where $f(z)$ is an entire analytic function and $F_1(a)$, $F_2(a)$ are some functions of a. The validity of this equation for all z, a is possible only if $F_1(a)=F_2(a)\equiv 0$ (if $f(z)$ has a zero, this follows immediately. The case when $f(z)$ has no zeros is also trivial). Thus,

$$\Phi(a)=\frac{1}{i\rho^2}\int_0^a\left(\bar{\zeta}\zeta'-\zeta\bar{\zeta}'\right)d\tau,\qquad\exp\left[\frac{1}{\rho^2}\int_0^T\left(\bar{\zeta}\zeta'-\zeta\bar{\zeta}'\right)d\tau\right]=1,$$

and, therefore,

$$\frac{1}{i\rho^2}\int_0^T\left(\bar{\zeta}(\tau)\zeta'(\tau)-\zeta(\tau)\bar{\zeta}'(\tau)\right)d\tau=\frac{4S}{\rho^2}=2\pi N,$$

where S is the area of the domain, bounded by the contour $\zeta(t)$.

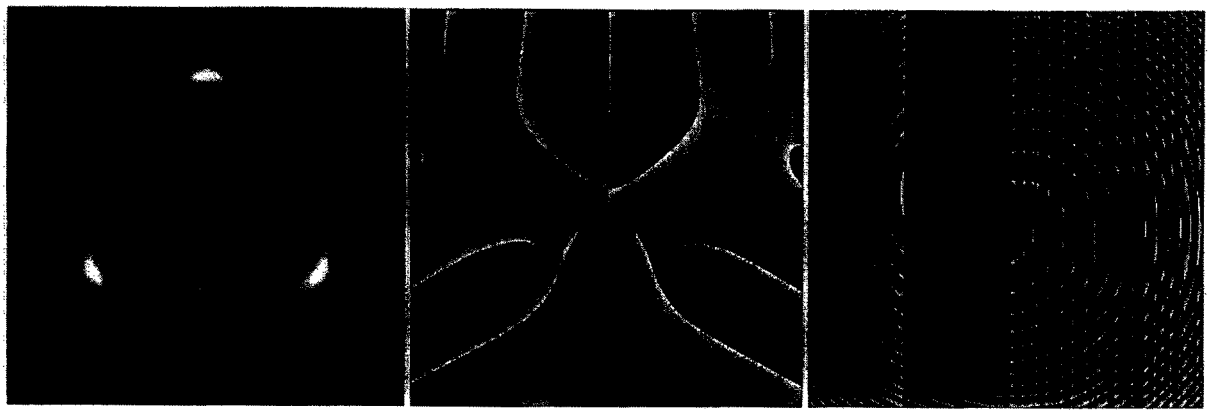

a b c

Fig. 6. Intensity (a), phase (b), and phase outside of the waist plane (c) of the beam in the shape of a triangular boundary. The triangle was modelled as the hypocycloid $\zeta(t) = i\nu(2e^{it} + \frac{1}{2}e^{-2it})$, $t \in [0, 2\pi]$. For the N-quantized curve, $\nu = \rho\sqrt{N/7}$. The present beam example corresponds to $N = 7$.

So, the beam intensity does not depend on the integration starting point a only for those curves for which the restricted domain area satisfies the quantization condition

$$S = \tfrac{1}{2}\pi\rho^2 N, \qquad N = 1, 2, \ldots. \tag{15}$$

We name the closed curves which satisfy Eq. (15) N-quantized ones, and spiral-type beams for these curves N-quantized beams (see Appendix A).

The quantization condition (15) comes out naturally from a consideration of closed polygonal lines as the limiting case of the additional phase agreement condition for the first and the last segments $\varphi_{n-1} = \varphi_0 + 2\pi N$ (see note 3 after Eq. (10)).

In Figs. 6 and 7, the quantized triangle-line beam and square-line beam are presented (compare Figs. 6c and 7c with the vortical axicon in Ref. [4]). Restricted domain areas are $\frac{7}{2}\pi\rho^2$ and $4\pi\rho^2$, respectively. In Figs. 6b

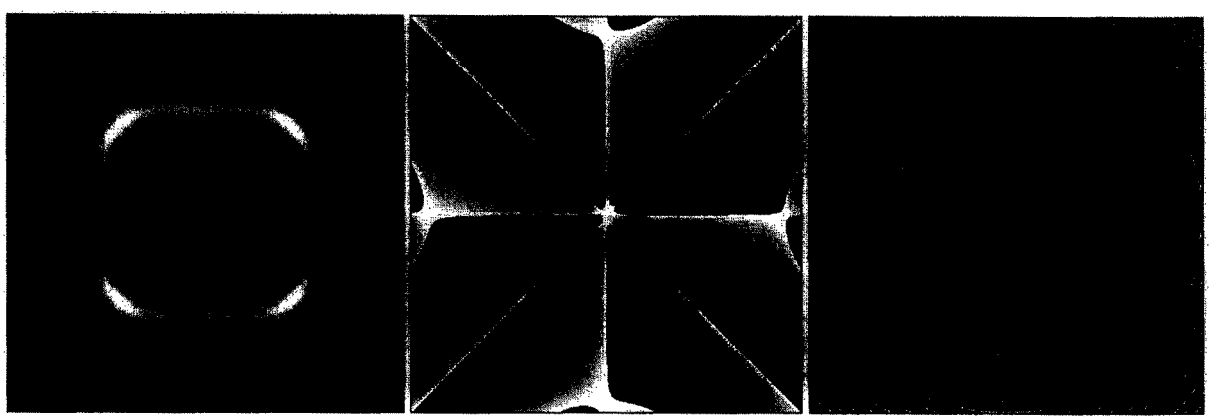

a b c

Fig. 7. Intensity (a), phase (b), and phase outside of the waist plane (c) of the beam in the shape of a square boundary. The square line was modelled as the epicycloid $\zeta(t) = i\nu(3e^{it} - \frac{7}{20}e^{-3it})$, $t \in [0, 2\pi]$. For the N-quantized curve, $\nu = \rho\sqrt{200N/3453}$. The present beam example corresponds to $N = 8$.

and 7b, the presence of phase dislocations (optical vortices) is seen; their numbers are 7 respectively.

b) Beam intensity and phase on the generating curve

There exists a characteristic property of quantized beams. Let $\zeta(t)$, $t\in[0, T]$ be a closed curve without self-crossings and let it satisfy conditions (15). Then $\mathscr{S}(\zeta(t_0), \bar{\zeta}(t_0)|\,\zeta(t), t\in[0, T])\neq 0$ for all $t_0\in[0, T]$. In other words, the entire function

$$f(z)=\int_0^T \exp\left[-\frac{\zeta(t)\bar{\zeta}(t)}{\rho^2}+\frac{2z\bar{\zeta}(t)}{\rho^2}+\frac{1}{\rho^2}\int_0^t\left(\bar{\zeta}\zeta'-\zeta\bar{\zeta}'\right)\mathrm{d}\tau\right]|\,\zeta'(t)\,|\,\mathrm{d}t$$

has no zeros on the quantized curve $z\in\{\zeta(t),\ t\in[0, T]\}$.

In order to analyze this assertion let us consider the asymptotic behavior of beams $\mathscr{S}(z, \bar{z}\,|\,\nu\zeta_1)$ for large values of the parameter ν/ρ by means of the saddle-point method [8]. Here ζ_1 is some closed 1-quantized curve without self-crossings. Here and below we will use a simpler notation $\mathscr{S}(z, \bar{z}\,|\,\zeta)$ for a spiral-type beam when the curve ζ does not need detailed description. Changing variables $z\mapsto\nu z$, we have

$$\mathscr{S}(\nu z,\nu\bar{z}\,|\,\nu\zeta_1)=\nu\int_0^T\exp\left(-\nu^2P(t)/\rho^2\right)|\,\zeta_1'(t)\,|\,\mathrm{d}t, \tag{16}$$

where $P(t)=z\bar{z}-2z\bar{\zeta}_1(t)+\zeta_1(t)\bar{\zeta}_1(t)-\int_0^t(\bar{\zeta}_1\zeta_1'-\zeta_1\bar{\zeta}_1')\,\mathrm{d}\tau$.

The saddle-point equation $P'(t)=2\bar{\zeta}_1'(t)(\zeta_1(t)-z)=0$ has solutions only for $z\in\{\zeta_1(t),\ t\in[0, T]\}$ as a result of the absence of singular points ($\zeta_1'(t)\neq 0$ for all t) and self-crossings ($\zeta_1(t_1)\neq\zeta_1(t_2)$ for $t_1, t_2\in(0, T)$ and $t_1\neq t_2$). Let $z=\zeta_1(t_0)$ for some $t_0\in[0, \mathrm{T}]$, and $\nu=\sqrt{n}\gg\rho$. Then $\sqrt{n}\,\zeta_1$ is an n-quantized curve and the integrand in (16) is a T-periodic function. Then Eq. (16) may be written as

$$\mathscr{S}\left(\sqrt{n}\,z,\ \sqrt{n}\,\bar{z}\,|\,\sqrt{n}\,\zeta_1\right)=\sqrt{n}\int_{t_0-T/2}^{t_0+T/2}\exp\left(-nP(t)/\rho^2\right)|\,\zeta_1'(t)\,|\,\mathrm{d}t.$$

Here we used the property $\int_0^T f(t)\,\mathrm{d}t=\int_a^{a+T}f(t)\,\mathrm{d}t$, which is valid for any T-periodic function. Since $t=t_0$ is the only (and simple) saddle point, then

$$\mathscr{S}\left(\sqrt{n}\,\zeta_1(t_0),\ \sqrt{n}\,\bar{\zeta}_1(t_0)\,|\,\sqrt{n}\,\zeta_1\right)=\sqrt{\pi}\,\rho\cdot\exp\left[\frac{n}{\rho^2}\int_0^{t_0}\left(\bar{\zeta}_1\zeta_1'-\zeta_1\bar{\zeta}_1'\right)\mathrm{d}\tau\right]+\mathrm{O}\left(\frac{1}{n/\rho^2}\right). \tag{17}$$

From (17) it is seen that the intensity at $n/\rho^2\to\infty$ tends to the nonzero constant $\pi\rho^2$, and hence the inequality $\mathscr{S}(\sqrt{n}\,\zeta_1(t_0), \sqrt{n}\,\bar{\zeta}_1(t_0)\,|\sqrt{n}\,\zeta_1)\neq 0$ is valid starting at some n (which, of course, depends on the shape of the curve $\zeta_1(t)$). It should be noted that with growing n/ρ^2, the intensity distribution on the curve $\sqrt{n}\,\zeta_1(t)$ becomes more and more uniform, and the absence of saddle points for $z\notin\{\zeta_1(t),\ t\in[0, T]\}$ leads to an intensity decrease away from the curve $\sqrt{n}\,\zeta_1(t)$. So, the asymptotic behavior of the intensity of a spiral-type beam provides the mathematical basis for the expression "a beam in the shape of the curve $\zeta(t)$".

For $\nu\neq\sqrt{n}$ (i.e. for a nonquantized curve $\nu\zeta_1(t)$) the asymptotic estimate is similar to Eq. (17) if the point t_0 is not near the boundary points $t=0$ or $t=T$. However, if $t_0=T$ or $t_0=0$, then the integrand in (16) is not a T-periodic function and the change of integration segment $[0, T]$ into $[t_0-\frac{1}{2}T,\ t_0+\frac{1}{2}T]$ is impossible. For this reason the points $t=0$ and $t=T$ should be considered as two different solutions of the saddle-point equation, and the asymptotic estimate in this case is

$$\mathscr{S}\left(\nu\zeta_1(T),\nu\bar{\zeta}_1(T)\,|\,\nu\zeta_1\right)=\frac{1}{2}\sqrt{\pi}\,\rho\left\{1+\exp\left[\frac{\nu^2}{\rho^2}\int_0^T\left(\bar{\zeta}_1\zeta_1'-\zeta_1\bar{\zeta}_1'\right)\mathrm{d}\tau\right]\right\}+\mathrm{O}\left(\frac{1}{\nu^2/\rho^2}\right).$$

From this equation it is seen that at $\nu\neq\sqrt{n}$, the intensity on the curve $\nu\zeta_1(t)$ does not tend to $\pi\rho^2$ at $\nu/\rho\mapsto\infty$

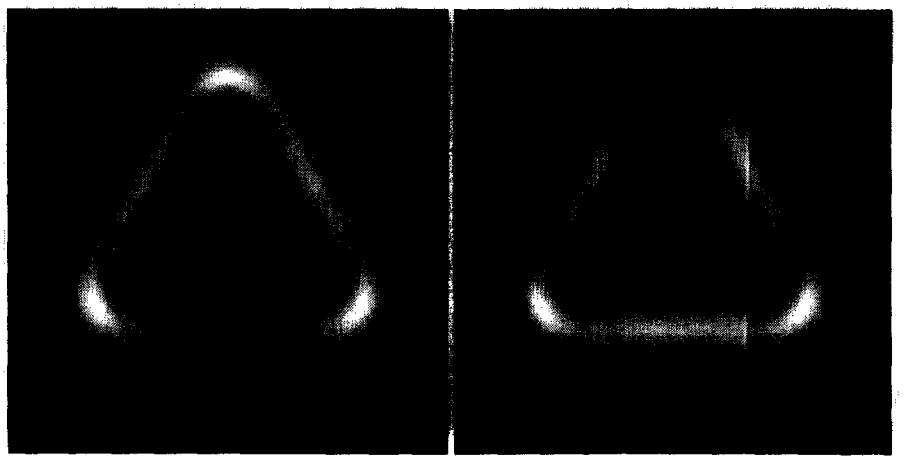

a b

Fig. 8. Spiral-type beam intensities for the nonquantized triangle curve $\zeta(t) = 1.0425i\rho(2e^{it} + \frac{1}{2}e^{-2it})$ for two integration starting points. Integration segments are $t \in [-\pi, \pi]$ (a) and $t \in [0, 2\pi]$ (b).

and, moreover, the position of the intensity nonuniformity point on the curve $\nu\zeta_1(t)$ is defined by the start of the integration interval. Fig. 8 illustrates the change of the intensity distribution of nonquantized beams in a triangle shape for two different starting points of the integration interval.

The asymptotic nature of the formulae found should be noted once more. For any fixed ν it is not difficult to find an example of a curve for which the second term in the expansions is comparable to the first. However, the preceding investigation shows the validity of the inequality $\mathscr{S}(\sqrt{n}\,\zeta_1(t_0), \sqrt{n}\,\bar{\zeta}_1(t_0) | \sqrt{n}\,\zeta_1) \neq 0$ for all $n \geqslant 1$. At present we have no rigorous mathematical proof of this assertion.

c) The number of zeros inside the generating curve region

Let us consider now the phase gradient circulation of a quantized beam $\mathscr{S}(z, \bar{z} | \sqrt{N}\,\zeta_1) = \sqrt{I}\,e^{i\varphi}$ along the contour C, described by the curve $\sqrt{N}\,\zeta_1(t)$. From Refs. [1, 3] it follows that

$$\oint_C \nabla\varphi \, d\mathbf{r} = 2\pi \sum_n \operatorname{sign} \operatorname{rot}_0 \mathbf{j}(z_n),$$

where

$$\operatorname{rot}_0 \mathbf{j} = \frac{1}{k}\left(\frac{\partial I}{\partial x} \cdot \frac{\partial \varphi}{\partial y} - \frac{\partial I}{\partial y} \cdot \frac{\partial \varphi}{\partial x}\right) = \frac{1}{k}[\nabla I, \nabla\varphi]_l$$

is the longitudinal component of the curl of the light energy flux field $\mathbf{j}$ and the summation is taken over all zeros z_n of the spiral-type beam which are placed inside the contour C, zero orders taken into account. If a zero z_n is nonsimple, then the sign of $\operatorname{rot}_0 \mathbf{j}(z_n)$ is defined as $\lim_{z \to z_n} \operatorname{sign} \operatorname{rot}_0 \mathbf{j}(z)$. For spiral-type beams (13), $\operatorname{sign} \operatorname{rot}_0 \mathbf{j}(z_n) = -\operatorname{sign}\, \theta_0 = 1$ (see Appendix A), and we have

$$\oint_C \nabla\varphi \, d\mathbf{r} = 2\pi N_0,$$

where N_0 is the number of zeros of the beam $\mathscr{S}(z, \bar{z} \mid \sqrt{N}\zeta_1)$ inside the contour C, zero orders taken into account.

Here we show that for quantized beams

$$N_0 = N. \tag{18}$$

As $N = 2S/\pi\rho^2$, (18) links a quantized beam number of zeros inside the domain bounded by the generating curve with the area of this domain. To prove this, let us first consider the construction of spiral-type beams for a circumference. Using Eq. (13) and removing a multiplicative constant, we have

$$\mathscr{S}(z, \bar{z} \mid Re^{it}, t \in [0, 2\pi]) = \exp(-z\bar{z}/\rho^2) \sum_{n=0}^{\infty} \frac{\sin(2R^2/\rho^2 - n)\pi}{2R^2/\rho^2 - n} \cdot \frac{(-2zR/\rho)^n}{n!}.$$

From the quantization condition for the circumference $S = \pi R^2 = \frac{1}{2}\pi\rho^2 N$ it follows that $2R^2/\rho^2 = N$ and the expansion is reduced to the Nth term:

$$\mathscr{S}\left(z, \bar{z} \mid \rho\sqrt{\tfrac{1}{2}N}\, e^{it}, t \in [0, 2\pi]\right) = \exp(-z\bar{z}/\rho^2) z^N. \tag{19}$$

Thus, quantized spiral-type beams for a circumference are the well-known Laguerre–Gaussian beams. The validity of Eq. (18) in this case is evident.

Let us suppose now that there is some N-quantized curve $\hat{\zeta}(t)$ for which Eq. (18) is not satisfied. Then we can construct a parametric set of curves $\zeta(t, c)$, which starts at the N-quantized circumference $\zeta(t, 0) = \sqrt{\frac{1}{2}N}\, e^{it}$, finishes at $\zeta(t, 1) = \hat{\zeta}(t)$, and has a fixed area of the interior region $S = \frac{1}{2}\pi\rho^2 N$ for every curve $\zeta(t, c)$. This ensures the validity of the quantization condition (15) for all $c \in [0, 1]$ under continuous deformation of the circumference. On the other hand, the spiral-type beam for the circumference satisfies Eq. (18), but the spiral-type beam for the curve $\hat{\zeta}(t)$ does not satisfy Eq. (18). Then for some c the number of zeros of the N-quantized beam $\mathscr{S}(z, \bar{z} \mid \zeta(t, c))$ changes inside the contour $\zeta(t, c)$. As for the realization of changes in zero number of a spiral-type beam with changes in the generating curve the following arguments may be used. Spiral-type beam zeros are zeros of corresponding analytic functions, and from the maximum modulus principle [9] it follows that an analytic function modulus has no minimum inside a region, except when the minimum is a zero of the function. Therefore, no zero can arise from a nonzero minimum of the function modulus or transform into the minimum inside the contour when changing the parameter c, because no such minimum for an analytic function exists. Thus, the number of zeros changes as a result of a zero moving into or out of the region bounded by the curve $\zeta(t, c)$. But in this case there is a c parameter value c_0 for which the spiral-type beam $\mathscr{S}(z, \bar{z} \mid \zeta(t, c_0))$ has a zero on the contour $\zeta(t, c_0)$. As has been noted above, this situation for quantized beams is impossible. So, for a quantized beam the number of optical vortices inside the domain bounded by the generating curve depends on the domain area, but not its shape. Hence it follows that under a change of area, for example from $S = \frac{1}{2}\pi\rho^2 N$ to $S = \frac{1}{2}\pi\rho^2(N+1)$, the beam zero number inside the generating curve region increases as a result of the intrusion of a zero from the outside. In Fig. 9 an evolution of a spiral-type beam for the circumference $\zeta(t) = Re^{it}$, $t \in [0, 2\pi]$ at $2R^2/\rho^2 \in [4.0, 5.0]$ is presented and a process of zero intrusion into the contour is visible. As it has already been noted, a zero intrusion zone is defined by the integration beginning [4].

[4] For the quantum-mechanical analog — ground state in a magnetic field — a noninteger value of $2S/\pi\rho^2$ corresponds to a nonquantized magnetic flux through the contour $\zeta(t)$: $\Phi = (2\pi\hbar c/|e|)N + \varepsilon$ and the situation has a certain resemblance with the Aharonov–Bohm effect [10].

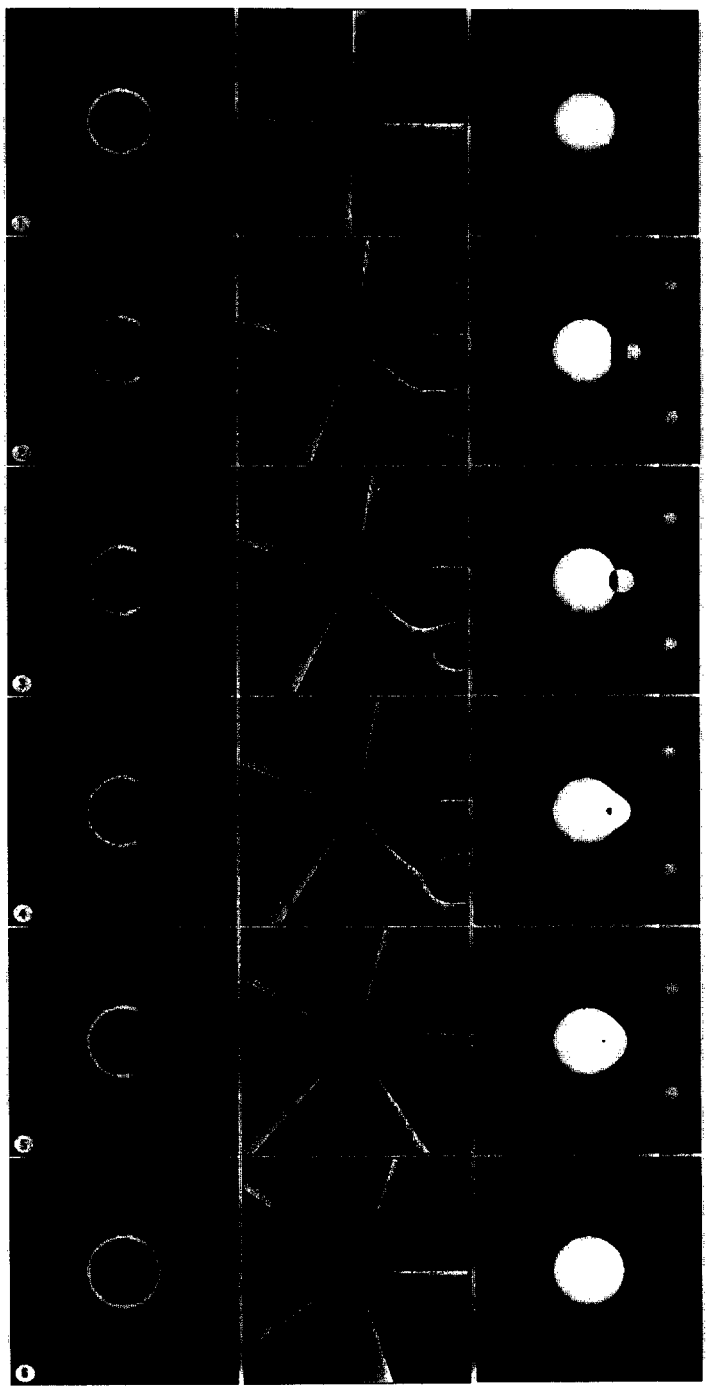

Fig. 9. Spiral-type beam evolution when changing the radius of the generating circumference: intensity (a), phase (b), and sign of $\mathrm{rot}_0 \mathbf{j}$ (c). Black corresponds to negative values of $\mathrm{rot}_0 \mathbf{j}$ and white to positive values.

5. Experiment

a) Amplitude-phase mask method

Experimental realization of the beams (13) was done in the following way. Amplitude halftone masks for amplitude and phase of a spiral-type beam were calculated by computer and produced by a photoplotter (resolution 1024×1024 pixels on a 10×10 mm^2 square). An amplitude mask for the phase was used to create a phase element on dichromated gelatin. Combination of the masks for amplitude A and phase P gives the necessary amplitude–phase distribution. We realized a triangle-line spiral-type beam outside the waist plane (cf. Figs. 6a and 6c; the wave front curvature is 0.002 mm^{-1}). The spatial frequency of the phase distribution in Fig. 6c is higher than that in Fig. 6b and there is an increase of the diffraction efficiency with the phase element on dicromated gelatin. The experimental setup is shown in Fig. 10. The beam from a laser L lights up the amplitude-phase element AP (the element has been rotated by 90° with respect to the distribution shown in Fig. 6). Lens 3 ($f = 250$ mm) focuses diffraction orders $+1$, 0 and -1 in the $+1$, 0 and -1 planes, respectively. Diffraction efficiencies in these orders are $\eta_1 : \eta_0 : \eta_{-1} \approx 10:7:3$, $\eta_1 \approx 40\%$. The intensity distribution structure is shown schematically at the bottom of Fig. 10. In orders $+1$ and -1, spiral-type beams rotate opposite to each other: $\mathscr{S}_{+1} = \exp(-z\bar{z})f(z)$, $\mathscr{S}_{-1} = \exp(-z\bar{z})\overline{f(z)}$. An ordinary diffraction pattern in the amplitude transparency A may be observed in the zero order. This field is not a spiral-type beam and when focused in plane 0 the field does not conserve its structure. In Fig. 11 an experimental distribution of intensity in diffraction order $+1$ is shown in plane $+1$.

b) Astigmatic transformation method

Now we consider another and not so evident way of realization of spiral-type beams. In Ref. [11], the transformation of Hermite–Gauss beams into Laguerre–Gauss beams with the help of astigmatic optics was presented. A particular case of this transformation is

$$\iint_{\mathbb{R}^2} \exp(-\mathrm{i}(x\xi + y\eta) + 2\mathrm{i}\xi\eta)\mathscr{H}_{n,0}(\xi, \eta)\,\mathrm{d}\xi\,\mathrm{d}\eta = \frac{\pi}{\sqrt{2}}(-2\mathrm{i})^n \exp\left(-\tfrac{1}{4}\mathrm{i}xy\right)\mathscr{L}_{0,n}\left(\frac{x}{\sqrt{8}}, \frac{y}{\sqrt{8}}\right).$$

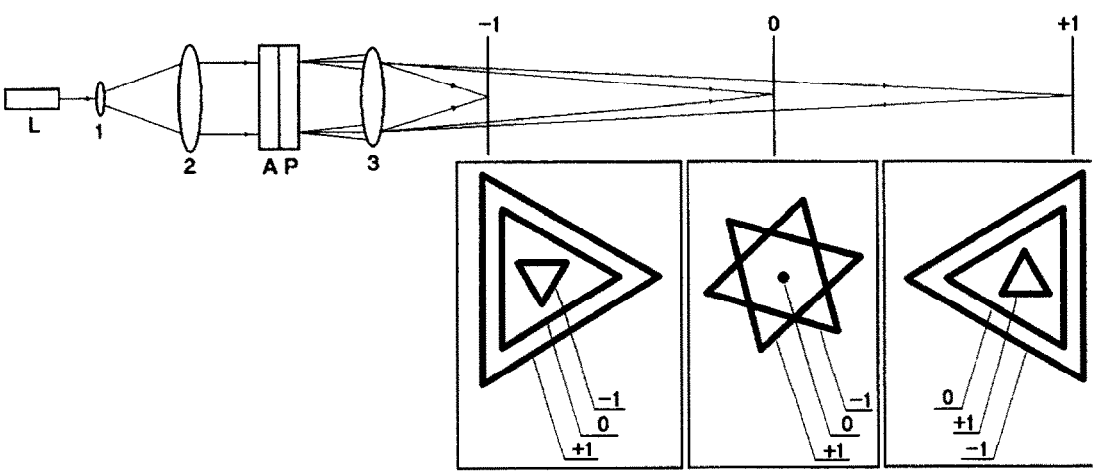

Fig. 10. Experimental setup for the synthesis of the triangle-line spiral-type beam.

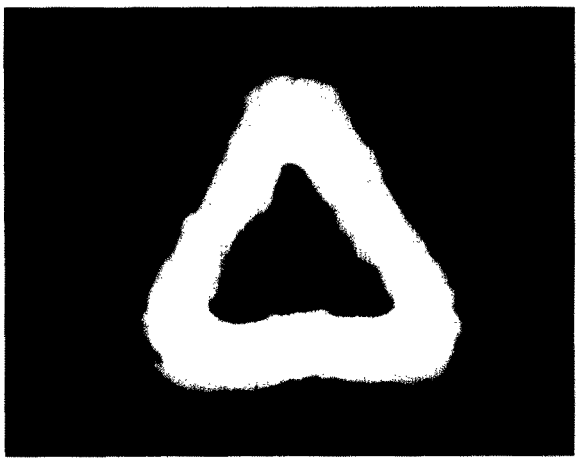

Fig. 11. Experimental intensity distribution of triangle-line spiral-type beam (+1 diffraction order).

This equation offers a possibility to synthesize spiral-type beams $\exp(-x^2-y^2)(x+\mathrm{i}y)^n$ and may be generalized in the following way:

$$\iint_{\mathbb{R}^2}\exp\left(-\mathrm{i}(x\xi+y\eta)+\frac{2\mathrm{i}\xi\eta}{\rho^2}-\frac{\eta^2}{\rho^2}\right)g\left(\frac{\xi}{\rho}\right)\mathrm{d}\xi\,\mathrm{d}\eta$$

$$=\sqrt{\pi}\,\rho^2\exp\left(-\tfrac{1}{4}\mathrm{i}\rho^2xy\right)\mathscr{S}(\rho(x+\mathrm{i}y),\rho(x-\mathrm{i}y)), \tag{20}$$

where $g(\xi)\in L_2(\mathbb{R})$ and the spiral-type beam $\mathscr{S}(z,\bar{z})$ is

$$\mathscr{S}(z,\bar{z})=\exp\left(-\tfrac{1}{8}z\bar{z}+\tfrac{1}{8}z^2\right)\int_{\mathbb{R}}\exp(-\xi^2-\mathrm{i}z\xi)g(\xi)\,\mathrm{d}\xi.$$

Eq. (20) suggests the following experimental procedure to synthesize spiral-type beams: a) form a light field $\exp(-\eta^2/\rho^2)g(\xi/\rho)$ for some function $g(\xi)$, b) perform an astigmatic transformation and c) compensate for the astigmatic factor after the transformation.

For example, if $g(\xi)=\mathrm{rect}(\xi/a)$, then a realized "segment"-beam is similar to the beam presented in Fig. 2. If $g(\xi)=\mathrm{rect}(\xi/a)\sum_{n=-N}^{N}\mathrm{e}^{\mathrm{i}n\omega\xi}$ then a realized spiral-type beam has the form of $2N+1$ parallel vertical "segment"-beams:

$$\mathscr{S}_N(z,\bar{z})=\sum_{n=-N}^{N}\exp\left(-\tfrac{1}{8}z\bar{z}+\tfrac{1}{8}z^2\right)\int_{-a}^{a}\exp(-\xi^2-\mathrm{i}\xi(z-n\omega))\,\mathrm{d}\xi. \tag{21}$$

At $\omega\sim\omega_0=2\sqrt{\pi}$, neighboring beams stick together and beam (21) looks like a zero lattice symmetrical in x and y (see Fig. 12). The frequency ω_0 may be deduced from the following consideration. At $a\gg 1$ and $N\to\infty$ the beam (21) may be written in the form

$$\mathscr{S}_\infty(z,\bar{z})=\sqrt{\pi}\exp\left(-\tfrac{1}{8}z\bar{z}-\tfrac{1}{8}z^2\right)\sum_{n=-\infty}^{\infty}\exp\left(-\tfrac{1}{4}\omega^2n^2+\tfrac{1}{2}\omega zn\right).$$

The last series is the theta-function ϑ_3. From the Poisson formula for this theta-function [12],

$$\sum_{n=-\infty}^{\infty}\exp(-\pi n^2+2\mathrm{i}nz)=\exp(-z^2/\pi)\sum_{n=-\infty}^{\infty}\exp(-\pi n^2+2nz)$$

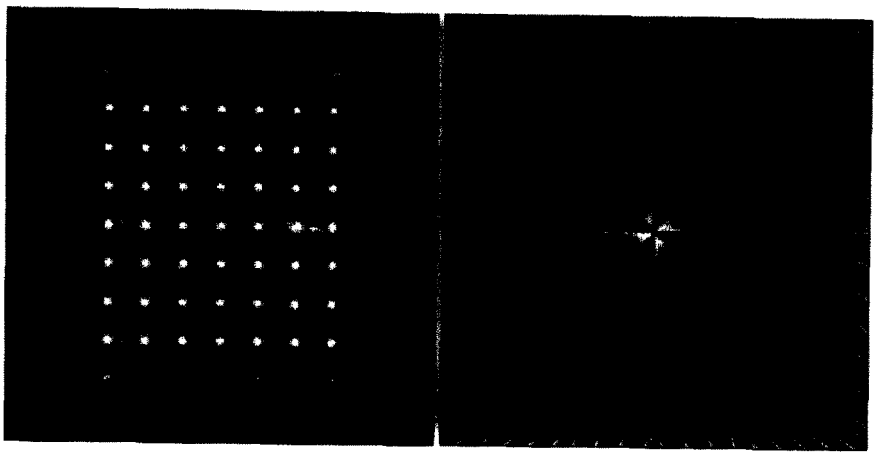

a b

Fig. 12. Intensity (a) and phase (b) of a spiral-type beam in the shape of a zero lattice (numerical experiment).

at $\omega = \omega_0$, and we have symmetry and periodicity of the intensity:

$$|\mathscr{S}_\alpha(z, \bar{z})|^2 = |\mathscr{S}_\infty(\mathrm{i}z, -\mathrm{i}\bar{z})|^2 = |\mathscr{S}_\infty(z+\omega_0, \bar{z}+\omega_0)|^2 = |\mathscr{S}_\infty(z+\mathrm{i}\omega_0, \bar{z}-\mathrm{i}\omega_0)|^2.$$

We realized the beam (21) using a Dammann grating with spatial frequency ω_0 as a multiplication element. The experimental setup is shown in Fig. 13. A laser beam is collimated by spherical lenses 1, 2. Cylindrical lenses 3, 4 compress the beam in one dimension and together with spherical 5 and cylindrical 6 form a field $\exp(-\eta^2/\rho^2)\,\mathrm{rect}(\xi/a)\exp(2\mathrm{i}\xi\eta/\rho^2)$ in the plane of diffraction grating 7, which gives 17 orders of equal intensity (see theory and experiment in Ref. [11]). Behind the grating, the astigmatic transformation (20) is realized in the Fraunhofer zone and the intensity distribution of the output field looks like a zero lattice. Remaining astigmatism in the Fraunhofer zone is compensated by two cylindrical lenses, the long-focus positive 8 and the negative 9. The reference beam is used for interference visibility of the spiral-type beam phase on the screen 10. In Fig. 14 the results of the experiment are shown. As can be seen in Fig. 14b, the fringe ramifies in each isolated zero that corresponds to the presence of a phase singularity. The curl values of the light energy

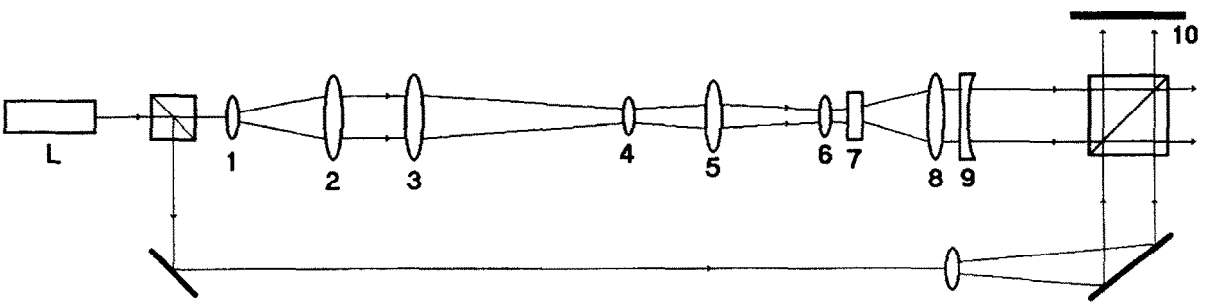

Fig. 13. Experimental setup for the synthesis of the beam in the shape of a zero lattice.

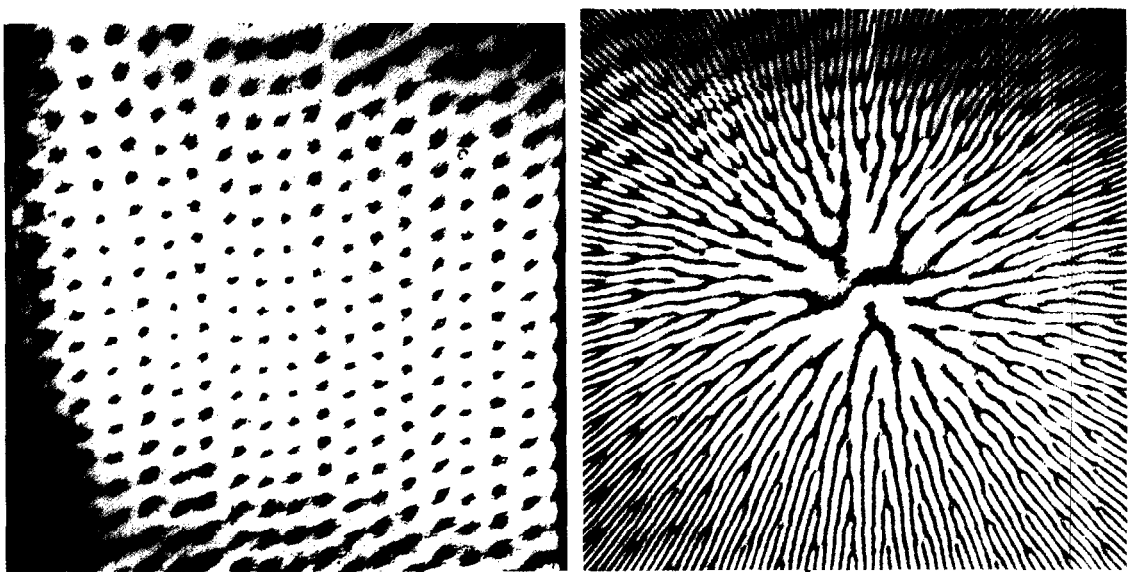

Fig. 14. A zero lattice beam: intensity (a) and pattern of interference between this beam and a reference beam (b).

flux field have the same sign in every intensity zero. The distortion of the experimental lattice structure in comparison with the theoretical distribution shown in Fig. 12 is the result of some residual aberrations.

A more general method to form spiral-type beams (1) which is similar to the above one may be deduced from results in Ref. [11]. As an example, let us consider an astigmatic transformation of a spiral-type beam (13):

$$\iint_{\mathbb{R}^2} \exp\left(-\mathrm{i}(x\xi+y\eta)+\frac{2\mathrm{i}\xi\eta}{\rho^2}\right)\mathscr{S}(\xi+\mathrm{i}\eta,\ \xi-\mathrm{i}\eta\,|\,\zeta)\,\mathrm{d}\xi\,\mathrm{d}\eta=\frac{\pi\rho^2}{\sqrt{2}}\exp\left(-\tfrac{1}{4}\mathrm{i}\rho^2xy-\tfrac{1}{8}\rho^2x^2\right)h(\rho y\,|\,\zeta),$$

where

$$h(\rho y\,|\,\zeta)=\exp\left(-\tfrac{1}{8}\rho^2y^2\right)\int_0^T\exp\left[-\frac{\bar{\zeta}^2(t)}{\rho^2}-\frac{\zeta(t)\bar{\zeta}(t)}{\rho^2}+y\bar{\zeta}(t)+\frac{1}{\rho^2}\int_0^t\left(\bar{\zeta}\zeta'-\zeta\bar{\zeta}'\right)\mathrm{d}\tau\right]|\,\zeta'(t)\,|\,\mathrm{d}t. \tag{22}$$

It is easy to see that all information about the spiral-type beam structure is contained in the integral part of Eq. (22), which is a function of one variable. Therefore, this function implements an original one-dimensional coding of the planar curve $\zeta(t)$ and we have the following method to create spiral-type beams: a) synthesize a one-dimensional amplitude–phase element $h(\rho y\,|\,\zeta)$, b) "restore" the intensity of the spiral-type beam with the help of an astigmatic gaussian beam $\exp(-\frac{1}{8}\rho^2(x^2+2\mathrm{i}xy))$ in the far diffraction zone or in the Fourier plane. In Fig. 15 an example of this amplitude–phase element used to synthesize a "triangle"-beam is shown (cf. Fig. 6). The one-dimensional structure of this element permits the use of all capabilities of microlithography and, hence, this method may be preferable for technology tasks.

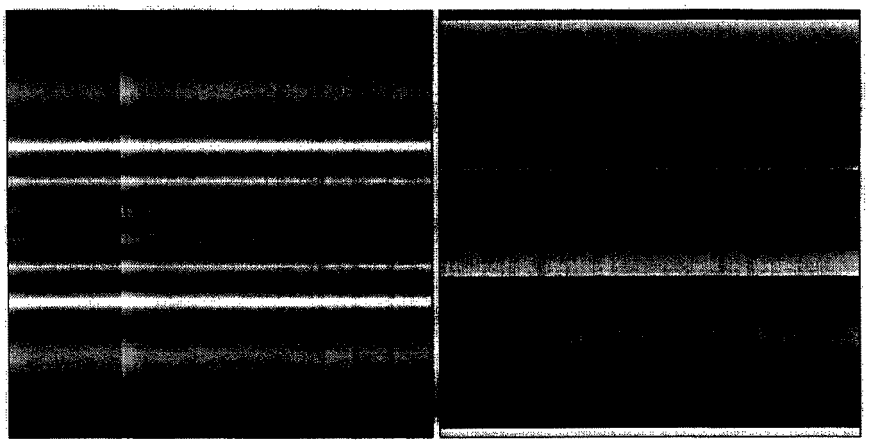

a b

Fig. 15. Amplitude (a) and phase (b) of the one-dimensional optical element $h(\rho y)\mathrm{i}\rho(2\mathrm{e}^{\mathrm{i}t}+\frac{1}{2}\mathrm{e}^{-2\mathrm{i}t})$, $t\in[0,2\pi]$, for astigmatic synthesis of the triangle-line spiral-type beam (cf. Fig. 6).

Experimental realization of spiral-type beams by means of one-dimensional elements is planned to be published later.

6. Discussion and conclusions

The main results of this work can be summarized as follows:
(i) a family of laser beams with predetermined intensity shape was found (in particular, the shape of an arbitrary curve, be it closed or open);
(ii) a relation between this beam family and a known quantum-mechanical situation — ground states of a charged particle in a uniform magnetic field — was discovered;
(iii) each beam with the topology of a closed curve without self-crossings satisfies a specific quantization condition. This property is similar to the quantization of the magnetic flux field through the curve;
(iv) some methods of synthesis of spiral-type beams were proposed and an example of an amplitude–phase optical element to convert a gaussian beam into a beam with triangle-line topology has been calculated and realized in practice.

A few theoretical results concerning spiral-type beam optics are presented in Appendix B, but some questions (for example, the properties of spiral-type beams for closed curves with self-crossings) are not included. Spiral-type beam optics is a wide and active field, not fully covered by this article. Nevertheless, the tools described here for optical manipulations are various enough. In Fig. 16 an example of a beam with complex topology is presented. It illustrates all possibilities at our disposal by the time the article was written. In spite of the "man-made" form, it is as natural a solution of the Schrödinger equation as the Hermite–Gauss and Laguerre–Gauss modes.

One more relation between this work and quantum mechanics should be noted. It concerns the problem of mechanical action of light on atoms. Ponderomotive laser action may be used in various applications such as atomic and molecular beam control, isotope separation, spatial localization and formation of atom grids in light fields [13]. Spatially inhomogeneous light fields with a possibility to control not only the magnitude but also the structure of the action attract much attention. In this case the light field phase is as important as the intensity and

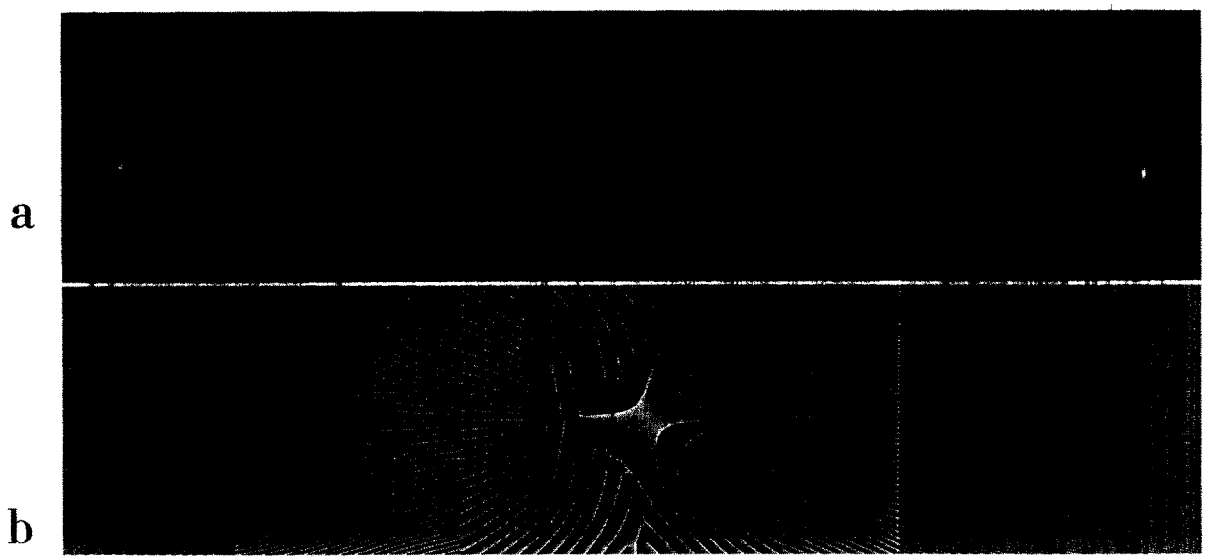

Fig. 16. Intensity (a) and phase (b) of a spiral-type beam with complex topology.

beam tools described in this work may be used for these tasks. For example, from Ref. [4] and the present work it follows that spiral-type beams are light fields with essentially nonzero curl of the light energy flux field $\mathrm{rot}_0 \mathbf{j} = [\nabla I, \nabla\varphi]_l/k$. On the other hand [13], a light field action on atoms which is linearly dependent on its velocity may be presented as a Lorentz force with some effective magnetic field $H_{\mathrm{eff}} \sim [\nabla I, \nabla\varphi]$ with a structure similar to $\mathrm{rot}_0 \mathbf{j}$, as was shown.

Finally it should be noted that, from the formal point of view, the basis of the theory of focus-wave modes and electromagnetic directed-energy pulses trains [14] is the Schrödinger equation and, therefore, the results of this work apply also in that field.

Acknowledgements

We thank N. Losevsky for preparation of the phase elements on dichromated gelatin.

Appendix A

The connection between paraxial optics and quantum mechanics has been considered by various authors (see, for example, Ref. [6]). What concrete quantum-mechanical situation corresponds to spiral-type beams? As was shown in Ref. [4], the equation for spiral-type beams in scaled polar coordinates R, φ is

$$\nabla^2 F + 4\mathrm{i}\theta_0 \partial F/\partial\varphi - 4F\left(R^2 - \gamma_0\right) = 0,$$

where $Re^{\mathrm{i}\varphi} = (x + \mathrm{i}y)\exp(\mathrm{i}\theta_0 \arg\sigma)/\rho|\sigma|$, $\sigma = 1 + 2\mathrm{i}l/k\rho^2$ and θ_0, γ_0 are constants. On the other hand ([7]), the Schrödinger equation for a charged particle with mass M and charge e in a uniform magnetic field H in ordinary polar coordinates R, φ is

$$\nabla^2\psi + 4\mathrm{i}\,\mathrm{sign}(eH)\partial\psi/\partial\varphi - 4\psi\left(R^2 - 2cME/\hbar|eH|\right) = 0,$$

where E is the particle energy. The equivalence of these equations for $\gamma_0 = 2cME/\hbar|eH|$, $\theta_0 = \mathrm{sign}(eH)$ is

seen. So, spiral-type beams (1) (in this case $\theta_0 = \pm 1$, $\gamma_0 = 1$) correspond to the particle wave functions of the ground state in the uniform magnetic field ($E = \hbar\,|\,eH\,|\,/2cM$). Eq. (15) corresponds to the quantized magnetic flow through the contour $\zeta(t)$: $\Phi = (2\pi\hbar c/|\,e\,|)N$. It should be noted that the above equations are the same in different coordinate systems.

Appendix B

Here we present some properties of spiral-type beams and the relation with certain transformations.

1. Let us return to the astigmatic transformation (20) and rewrite the obtained spiral-type beam $\mathscr{S}(z, \bar{z})$ in the form

$$\mathscr{S}(2\mathrm{i}z, -2\mathrm{i}\bar{z}) = \exp\left(-\tfrac{1}{2}z\bar{z}\right)\int_{\mathbb{R}} \exp\left(-\tfrac{1}{2}z^2 + 2z\xi - \xi^2\right) g(\xi)\,\mathrm{d}\xi = \exp\left(-\tfrac{1}{2}z\bar{z}\right) f(z).$$

Then we have the continuous counterpart of the Gabor expansion [15] of the function $g(\xi)$, in which the analytic function $f(z)$ is connected with $g(\xi)$ through an integral transformation with kernel $\exp(-\frac{1}{2}z^2 + 2z\xi - \xi^2)$. On the other hand, in quantum mechanics [5], the coordinate representation of the state $|\,q\rangle$ and the Fock–Bargman representation $\langle z\,|$ are connected by the integral transformation with kernel

$$\langle z\,|\,q\rangle = \frac{1}{\sqrt[4]{\pi\hbar}} \exp\left(-\frac{z^2}{2} + \frac{2zq}{\sqrt{2\hbar}} - \frac{q^2}{2\hbar}\right).$$

Thus, the astigmatic transformation (20) realizes a connection between two quantum-mechanical representations by optical methods.

2. Eq. (20) indicates the possibility of an optical realization of an analytic continuation of the Fourier image of the field $g(\xi)$ with the help of the astigmatic transformation. As an example for a finite field $g(\xi)$ with support $[-a, a]$, the action order is as follows. First, the field $g(\xi)$ is passed through the amplitude mask $\exp(-a^2 + \xi^2 - \eta^2)$ and the astigmatic phase element $\exp(2\mathrm{i}\xi\eta)$. Then an optical Fourier transformation is realized. The output field zeros are zeros of the analytic continuation of the Fourier image of the field $g(\xi)$. This optical analytic continuation may be used as the basis of the new phase retrieval method (see also Refs. [16,2,3]).

3. A symmetry of a closed curve appears in the properties of the corresponding spiral-type beams. Let $\zeta(t)$, $t \in [0, 2\pi]$ be parametrized by the polar angle and be stable under rotation by an angle $2\pi/M$, i.e. $\zeta(t + 2\pi/M) = \zeta(t)\exp(2\pi\mathrm{i}/M)$. Then the quantized spiral-type beams $\mathscr{S}_n(z, \bar{z})$ for the corresponding quantized curves $\zeta_n(t)$ have the following properties:

(i) $\mathscr{S}_n(z\mathrm{e}^{2\pi\mathrm{i}/M}, \bar{z}\mathrm{e}^{-2\pi\mathrm{i}/M}) = \mathscr{S}_n(z, \bar{z})\mathrm{e}^{2\pi\mathrm{i}n/M}$;

(ii) the point $z = 0$ is zero with order $n - [n/M]M$ of the beam $\mathscr{S}_n(z, \bar{z})$. If $n \geqslant M$, then other zeros within the contour $\zeta_n(t)$ are placed at corners of regular M-gons (one or several). For example, $M = 3$ for a hypocycloid $\zeta(t) = \mathrm{i}\rho(2\mathrm{e}^{\mathrm{i}t} + \frac{1}{2}\mathrm{e}^{-2\mathrm{i}t})$, $t \in [0, 2\pi]$. So, the beam $\mathscr{S}_7(z, \bar{z})$ has a prime zero $z = 0$ and 6 others at the corners of two regular triangles (see Fig. 6).

(iii) If $(n - m)/M$ is noninteger, then the beams $\mathscr{S}_n(z, \bar{z})$ and $\mathscr{S}_m(z, \bar{z})$ are orthogonal in the space $L_2(\mathbb{R}^2)$. To prove this, it is sufficient to note that

$$(\mathscr{S}_n, \mathscr{S}_m)_{L_2(\mathbb{R}^2)} = \int_0^{2\pi} \mathscr{S}_n\left(\zeta_m, \bar{\zeta}_m\right) \exp\left[-\frac{1}{\rho^2}\int_0^t \left(\bar{\zeta}_m\zeta_m' - \zeta_m\bar{\zeta}_m'\right)\mathrm{d}\tau\right] |\,\zeta_m'\,|\,\mathrm{d}t$$

$$= \int_0^{2\pi/M} \mathscr{S}_n\left(\zeta_m, \bar{\zeta}_m\right) \exp\left[-\frac{1}{\rho^2}\int_0^t \left(\bar{\zeta}_m\zeta_m' - \zeta_m\bar{\zeta}_m'\right)\mathrm{d}\tau\right] |\,\zeta_m'\,|\,\mathrm{d}t \sum_{k=0}^{M-1} e^{2\pi\mathrm{i}(n-m)k/M} = 0.$$

For example, M is an arbitrary integer for circumferences. So, in this case $(\mathscr{S}_n, \mathscr{S}_m)_{L_2(\mathbb{R}^2)} = 0$ for all $n \neq m$.

The integral equality is well-known as a particular case of the Laguerre–Gauss beam orthogonality (see Eq. (19)).

4. Evolution of the field $F(x, y, 0) = \exp(-\frac{1}{8}\rho^2 y^2)h(\rho x \mid \zeta)$ from (22) under propagation is given by

$$F(x, y, l) = \frac{k}{2\pi i l}\iint_{\mathbb{R}^2} \exp\left\{\frac{ik}{2l}\left[(x-\xi)^2 + (y-\eta)^2\right]\right\} F(\xi, \eta, 0)\, d\xi\, d\eta$$

$$= \frac{1}{\sigma}\exp\left(\frac{il\rho^4(x^2+y^2)}{32k|\sigma|^2}\right)\exp\left(-\frac{\rho^2 y^2}{8|\sigma|^2}\right)h\left(\frac{\rho x}{|\sigma|}\middle|\zeta e^{i\arg\sigma}\right), \tag{B.1}$$

where $\sigma = 1 + il\rho^2/4k$. Comparing (22) and (B.1) it is seen that the above field $F(x, y, l)$, with scale and phase factors neglected, is the astigmatic transformation of the spiral-type beam $\mathscr{S}(ze^{-i\arg\sigma}, \bar{z}e^{i\arg\sigma} \mid \zeta)$. This beam is deduced from the initial one by rotation over an angle $\arg\sigma$. The transformation (B.1) and corresponding astigmatic transformation have a geometrical interpretation. Following Ref. [11], let us consider the three-dimensional complex distribution

$$W(x, u, y) = \exp(-2ixu/\rho^2 - 2y^2/\rho^2)\mathscr{S}(x + iu, x - iu \mid \zeta).$$

The projection of this distribution on the plane $u = 0$ is

$$W_P(x, y) = \int_{\mathbb{R}} W(x, u, y)\, du = \sqrt{\pi}\,\rho \exp(-2y^2/\rho^2)h(4x/\rho \mid \zeta).$$

This projection is similar to $F(x, y, 0)$. If $W(x, u, y)$ is rotated around the y axis through angle $\arg\sigma$ then its projection on the plane $u = 0$ is equal to $F(x, y, l)$, if we neglect scale and phase factors. Therefore, the evolution of the field $F(x, y, l)$ under propagation looks like a change of the projection of $W(x, u, y)$ under rotation around the y axis.

References

[1] E. Abramochkin, V. Volostnikov and A. Malov, VINITI 3773-V87 (1987);
E. Abramochkin and V. Volostnikov, Optics Comm. 74 (1989) 139.
[2] E. Abramochkin and V. Volostnikov, Optics Comm. 74 (1989) 144.
[3] V. Volostnikov, J. Sov. Laser Research 11 (1990) 601.
[4] E. Abramochkin and V. Volostnikov, Optics Comm. 102 (1993) 336.
[5] A.M. Perelomov, Generalized coherent states and their applications (Springer, Berlin, 1986);
V.V. Dodonov and O.V. Man'ko, Invariants and evolution of nonstationary quantum systems (Nauka, Moscow, 1987).
[6] D. Marcuse, Light transmission optics (Van Nostrand Reinhold Company, New York, 1972).
[7] L.D. Landau and E.M. Lifshitz, Quantum mechanics (Nauka, Moscow, 1989).
[8] F.W.J. Olver, Asymptotics and special functions (Academic Press, New York, 1974).
[9] E.C. Titchmarsh, The theory of functions (University Press, Oxford, 1939).
[10] Y. Aharonov and D. Bohm, Phys. Rev. 115 (1959) 485.
[11] E. Abramochkin and V. Volostnikov, Optics Comm. 83 (1991) 123.
[12] E.T. Whittaker and G.N. Watson, A course of modern analysis (University Press, Cambridge, 1927).
[13] A.D. Kazantsev, G.I. Surdutovich and K.V. Yakovlev, Mechanical action of light on atoms (World Scientific, Singapore, 1990).
[14] J.N. Britinham, J. App. Phys. 54 (1983) 1179;
P.W. Ziolkowski, Phys. Rev. A 39 (1989) 2005.
[15] D. Gabor, Proc. Inst. Electr. Eng. 93 (1946) 429.
[16] J.W. Wood, M.A. Fiddy and R.E. Burge, Optics Lett. 6 (1981) 514.